The Nucleus ***59****, No. 1-2 (2022) 1-9*

www.thenucleuspak.org.pk

The Nucleus
ISSN 0029-5698 (Print)
ISSN 2306-6539 (Online)

Impact of Inner Dopants on Structural, Optical and Mechanical Properties of Unadulterated L-Threonine Manganese Acetate

N.I. Ahamed[1*], D.B. Anburaj[2], G. Nedunchezhian[1]

[1]*PG and Research Department of Physics, Thiru. Vi. Ka. Govt. Arts College, Thiruvarur, Tamil Nadu, India*

[2]*PG and Research Department of Physics, D.G. Govt. Arts College (W), Mayiladuthurai, Tamil Nadu, India*

ABSTRACT

In this work, equal molar ratio of L-Threonine and Manganese Acetate (LTMA) and 0.2 molar of Zn^{2+}, Cd^{2+} and Pb^{2+} doped LTMA single crystals were grown in aqueous solutions using slow evaporation technique. These crystals were subjected to various studies including single crystal X-ray diffraction, powder X-ray diffraction, FTIR, UV-vis, energy dispersive X-ray spectroscopy (EDX) and microhardness test. The cell length and interfacial angles α, β, and γ of the grown crystals were determined. EDX study confirms the placing of dopant ions Zn^{2+}, Cd^{2+} and Pb^{2+} in the host material LTMA. FTIR analysis reported the functional group and UV-vis was carried out to study the optical behavior of the grown crystals. UV-vis studies determined the increasing energy band gap from 4.6 eV to 6.5eV and transmittance spectrum determined the lower cutoff wavelength of the grown crystals as 267 nm for the pure LTMA and ~200 nm for the doped LTMA crystals. Mechanical behavior of the crystals was studied by Vicker's Microhardness study and their roughnesses were also reported.

Keywords: *Metallic Dopants, Single Crystal XRD, Ferroelectric, Nonlinear Optical Materials, Microhardness*

1. Introduction

Single crystals are the fundamental building blocks of the materials used in modern technology. Crystal growth has controlled phase transformation and implies important natures, properties and qualities in material science. Crystal growth technology has developed excellent crystals, in ever growing applications of the material in lasers, optical communication and data storage devices. Some single crystals are very important and essentiality for the advanced research and technologies in the future. Large size crystals are very important for the device fabrication using several fast growing techniques. The present day demand is for the large and high quality nonlinear optical (NLO) materials, ferroelectric, piezoelectric single crystals and magnetic materials with minimum defects [1, 2]. Synthesis of many crystals is a complicated process to attain notable materials for technological applications [3]. Crystal growth is an art of growing crystals based on scientific principles to facilitate high technological applications in lasers, semiconducting devices, computers, magnetic and optical devices and pharmaceuticals [4-9]. The growth of single crystals is both scientifically and technologically important. In this regard, amino acid based single crystals are very successful materials [10]. Researchers studied amino acids such as L-Alanine, L-Proline, L-Arginine, L-Histidine and L-Valine etc. [11-15]. Most of the recent exploration works have been done on semi natural crystals. Because of their wide optical applications, contrasted with different materials, amino corrosive blended natural crystal was intrigued to orchestrated. This material has qualified for the discovery of numerous natural NLO materials with high nonlinear nature and photonic applications. It can also be utilized in gems as precious stones. Like the semi natural precious stones, amino corrosive based semi natural gems have acceptable optical and non-direct optical natures. This single crystal can be developed with improved hardness and steadiness. In this reference, unadulterated L-Threonine single gem and L-Threonine based lithium chloride (LTLC), calcium chloride (LTCC), cadmium chloride (LTCC), manganese chloride (LTMC) single crystals were developed and examined [14-18]. Afterwards, L-threonine sulfate crystal like lithium sulfate (LTLS), potassium sulfate (LTKS), zinc sulfate (LTZS) and copper sulfate (LTCS) single crystals were also developed [19-22]. Similarly, L-threonine cadmium acetate (LTCA) and L-threonine zinc acetate (LTZA) single precious crystals were developed and investigated [23-24].

2. Materials and methods

2.1. Synthesis

AR grade chemicals of L-threonine and manganese (II) acetate tetra hydrate with ratio of 1:1 were taken in 10 ml distilled water. 0.2 M of zinc (II) acetate (ZnA), cadmium (II) acetate (CdA) and lead (II) acetate (PbA) were added in 1:0.8 molar ratio of L-threonine and manganese (II) acetate. All the prepared saturated solutions were filtered and then housed in a dust free atmosphere. The pure LTMA single crystal and Zn^{2+} doped LTMA, Cd^{2+} doped LTMA and Pb^{2+} doped LTMA single crystals were successfully grown at 30°C using slow evaporation technique.

After a period of 25 days, harvested single crystals of 10×3×2 mm^3 size pure LTMA single crystal, 10×4×2 mm^3 size of Zn^{2+} doped LTMA, 10×3×2 mm^3 size of Cd^{2+} doped LTMA and 10×3×2 mm^3 size of Pb^{2+} doped LTMA were grown as shown in Fig. 1.

The chemical formula for this process is given below:

Pure LTMA single crystal

$$C_4H_9NO_3+(CH_3COO)_2Mn.4H_2O$$

$$\rightarrow Mn[C_4H_9NO_3]^{+2}(CH_3COO)^{-}+4H_2O\uparrow \quad (1)$$

*Corresponding author: imthiiaz@yahoo.com

0.2M $(X)^{2+}$ doped LTMA single crystal

$$C_4H_9NO_3+8M(CH_3COO)_2.Mn.4H_2O+0.2M(CH_3COO)_2(X) \rightarrow (Mn_{0.8}[C_4H_9NO_3](X)_{0.2})^{+2}(CH_3COO)^{-}+ 4H_2O\uparrow \quad (2)$$

(Where X is substituted by Zn^{2+}/ Cd^{2+}/ Pb^{2+})

Fig. 1: As grown (a) pure LTMA (b) Zn^{2+} doped LTMA (c) Cd^{2+} doped LTMA (d) Pb^{2+} doped LTMA single crystals

3. Results and Discussion

This section deals with characterization techniques of the grown single crystals. These techniques help to study the qualitative nature of the grown single crystals. It investigates the details of the presence of chemicals and their performance inside the material. Behavior of a crystal varies importantly with its chemical compositions, dimensions, and imperfections or impurities. The study of its electronic applications, stable hardness **(**non-electrical**)**, thermo-gravimetric and optical properties was performed. The characterization of the grown pure LTMA and doped LTMA was performed by single crystal XRD, powder XRD, energy dispersive X-ray analysis (EDX), Fourier transform infrared spectroscopy (FTIR), and UV-visible absorbance spectral analysis.

In this investigation, the grown crystals were subjected to crystallographic analysis like X-ray diffraction (XRD) study to determine the crystal system and its lattice parameters. The EDX shows the presence of constituent elements in the prepared material. The functional groups and vibrational frequencies were identified using FTIR analyses. The UV-visible absorbance spectra were recorded to find out the cut-off wavelength and band gap of different compositions. The photoluminescence and second harmonic generation of the crystal for NLO applications were determined and microhardness test was performed to evaluate the mechanical strength of the material.

3.1. Single crystal X-ray diffraction analysis

Single crystal X-ray diffraction study was done to find the crystallinity and information about the unit cell of the grown crystals. It proves that all the pure and doped single crystals were the same (orthorhombic crystal type), which are categorized as non-centro-symmetric. The unit cell parameters for pure LTMA and Zn^{2+}doped LTMA, Cd^{2+} doped LTMA and Pb^{2+} doped LTMA single crystals are given in table 1. The volume of the pure LTMA becomes 530(4) $Å^3$ and all the doped crystals were increased to 538 $Å^3$ for Zn^{2+} doped LTMA, 540 $Å^3$ for Cd^{2+} doped LTMA and 540.8(4) $Å^3$ for Pb^{2+} doped LTMA.

3.2. Powder XRD analysis

The Powder XRD pattern of pure LTMA and Zn^{2+}, Cd^{2+} and Pb^{2+} doped LTMA single crystals were plotted as shown in Fig. 2. All the doped powder XRD patterns are clearly shown with different peaks of the dopants and the similarities and differences between the pure and doping crystals as shown in Fig. 2. The inner reagents of Zinc (II) acetate (ZnA), cadmium (II) acetate (CdA) and lead (II) acetate (PbA) were well mixed with manganese (II) acetate (MnA) with 0.2 M and 0.8 M ratios. This perfect mixture results that without changing the pure LTMA crystal structure, all Zn^{2+} doped LTMA, Cd^{2+} doped LTMA and Pb^{2+} doped LTMA single crystals also have the same orthorhombic structure. The *hkl* planes of the pure LTMA and Zn^{2+}, Cd^{2+} and Pb^{2+} doped LTMA single crystals with respective 2θ values are calculated and tabulated in tables 3, 4 and 5, respectively. Most of the peaks are differed with different 2θ values.

Therefore, 0.2 M dopant of Zn^{2+}, Cd^{2+} and Pb^{2+} doped LTMA single crystals, the first peaks remain the same as the maximum peak from the pure LTMA, which are 1163 amu and 1184 amu, 1029 amu and 1184 amu for Zn^{2+} doped LTMA, Cd^{2+} doped LTMA and Pb^{2+} doped LTMA single crystals.

Table 1: Lattice parameters of pure LTMA and Zn^{2+}, Cd^{2+} and Pb^{2+} doped LTMA single crystals

Lattice parameters	Pure LTMA	Zn^{2+} doped LTMA	Cd^{2+} doped LTMA	Pb^{2+} doped LTMA
a	5.106(19) Å	5.17 Å	5.14 Å	5.147(3) Å
b	7.721(19) Å	7.71 Å	7.72 Å	7.731(2) Å
b	13.45(4) Å	13.59 Å	13.60 Å	13.590(10) Å
α=β=γ	90°	90°	90°	90°
Volume	530(4) $Å^3$	538 $Å^3$	540 $Å^3$	540.8(4) $Å^3$
System	Orthorhombic	Orthorhombic	Orthorhombic	Orthorhombic
Space group	P_{212121}	P_{212121}	P_{212121}	P_{212121}

3.3. EDX analysis

Energy dispersive spectroscopy is a chemical technique measured by Quanta 200 FEG scanning electron microscope (Fig. 3). The interaction of the electron beam with the specimen in the scanning electron microscope produces X-rays. These X-rays determine the characteristic peaks of the element. This technique is used to find out the elemental composition of the sample. Elemental evaluation by the analytical microscopy may be accomplished with the help of analyzing the emitted radiations. All the crystals were subjected to energy dispersive analysis. Elements are determined and displayed as atomic percentile. Energies obtained correspond to the elements with positioning in pure and doped LTMA crystals are shown in Fig. 3(a), (b), (c), and (d). In EDX analysis, the presence of Mn^{2+} in pure LTMA single crystal was observed. In doped LTMA single crystals all the dopant (Zn^{2+}, Cd^{2+} and Pb^{2+}) were present. The values of EDX spectra are reported in table 6, 7, 8 and 9.

Table 2: hkl planes of pure LTMA single crystal

20	Intensity	hkl
4.0	1163	111
8.8	93	211
12.5	134	222
17.6	100	411
22.2	345	422
25.6	154	431
26.6	203	444
36.0	108	552
38.4	113	661

Table 3: hkl planes of Zn^{2+} doped Pure LTMA single crystal

2θ	Intensity	Hkl
4.1	1184	111
12.6	100	211
17.6	160	220
19.6	173	221
20.6	384	301
21.0	199	311
22.6	147	222
25.6	151	302
28.0	108	321
29.0	182	322
31.0	139	402
34.0	104	422
36.0	95.9	432
38.8	78.8	521
41.8	104.5	532

Table 4: hkl planes of Cd^{2+} doped Pure LTMA single crystal

2θ	Intensity	hkl
4.1	1029	111
13.1	230	211
18.2	157.4	311
20.2	256.7	222
20.6	235.0	321
21.5	187.8	322
22.2	174.8	331
22.9	230.7	421
23.5	144.9	422
23.9	200.8	500
28.6	252.4	521
29.2	157.0	440
35.0	93.3	442
37.3	127.6	543
39.0	100	551

3.4. Fourier Transform Infra-Red analysis

The FTIR spectrum of the pure and doped LTMA crystals was obtained as shown in Fig. 4. The placing of NH^{3+} is clearly identified in FTIR spectrum by the wide intense peak at 3169.25 cm^{-1} relating to the asymmetric vibration mode of NH^{3+}. The opposite symmetric vibration band lies at 3029.80 cm^{-1}. Both symmetric and asymmetric bending vibrations appear as 1417.94 cm^{-1} and 1629.28 cm^{-1}. CH symmetric deformation appears at 1346.04 cm^{-1}. NH^{3+} rocking, C-N rocking, C-C rocking and C-C-N rocking appearing at 1113.14 cm^{-1}, 1040.72 cm^{-1}, 932.53 cm^{-1}, 871.20 cm^{-1} and 769.77 cm^{-1} indicate COO^- bending, whereas 701.35 cm^{-1} and 560.11cm^{-1} indicate the COO^- wagging vibration and COO^- rocking deformation, respectively. NH^{3+} bending appears at 489.82 cm^{-1} and the OCO rocking frequency was found at 445.18 cm^{-1}.

Table 5: hkl planes of Pb^{2+} doped pure LTMA single crystal

2θ	Intensity	hkl
3.93	1178	111
12.5	134	211
17.6	100	222
22.2	345	411
25.6	154	422
26.6	203	431
36.0	108	444
38.4	113	552
44.9	176	661

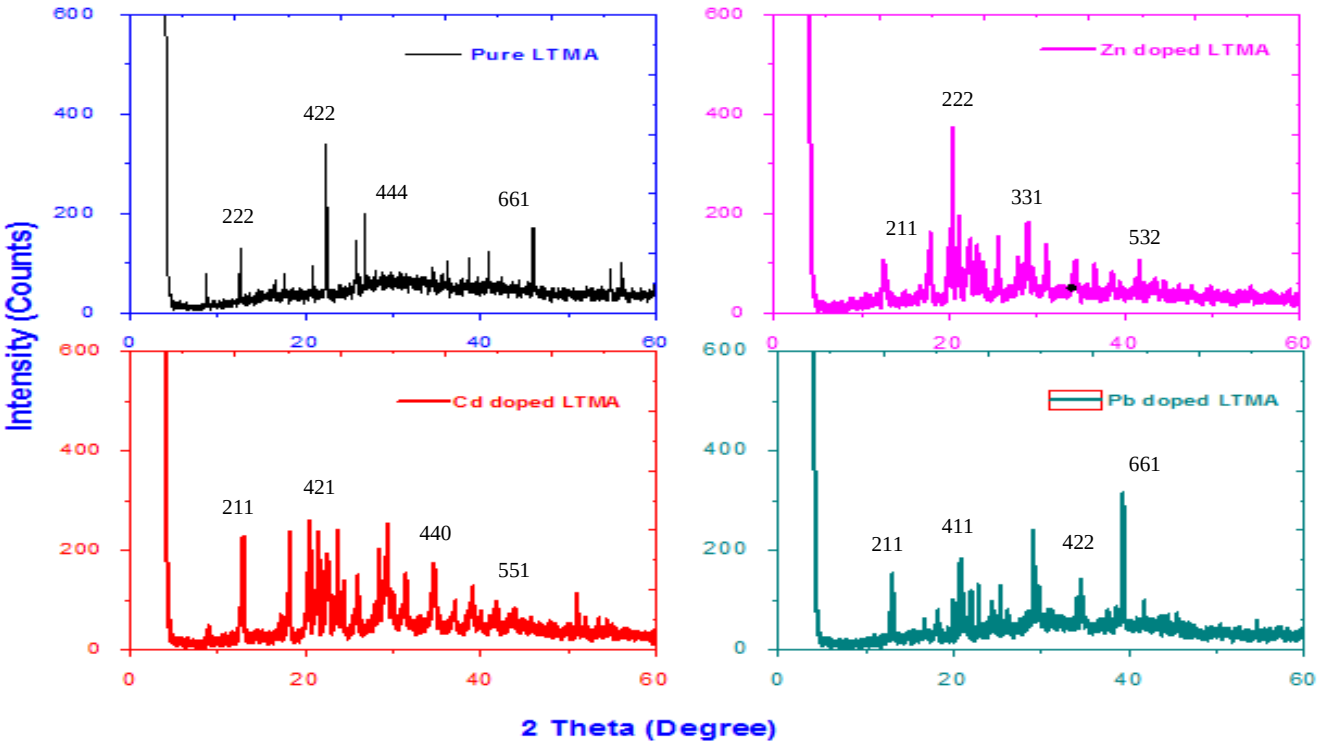

Fig. 2: XRD plotting of pure LTMA and Zn^{2+}, Cd^{2+} and Pb^{2+} doped LTMA

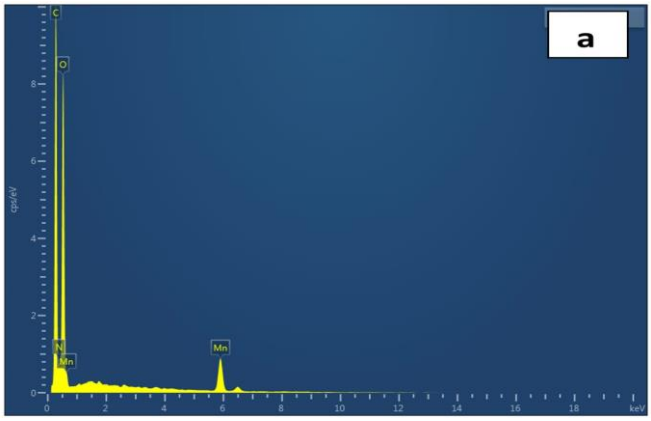

Fig. 3: Energy dispersive spectra of (a) pure LTMA

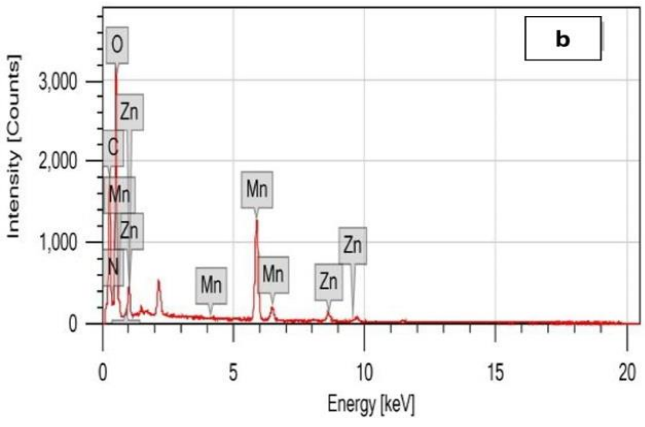

Fig. 4: Energy dispersive spectra of (b) Zn^{2+} doped LTMA

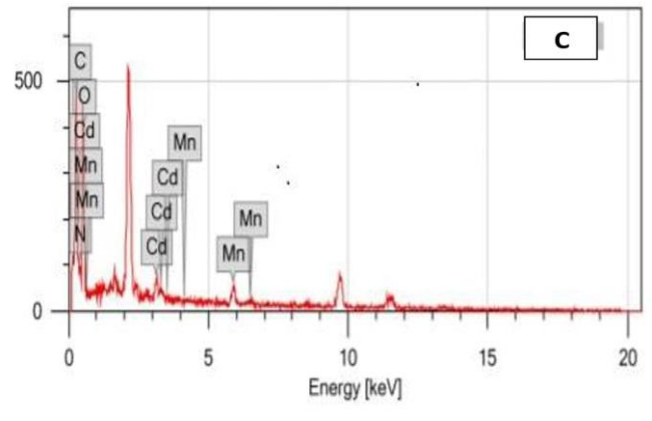

Fig. 5: Energy dispersive spectra of (c) Cd^{2+} doped LTMA

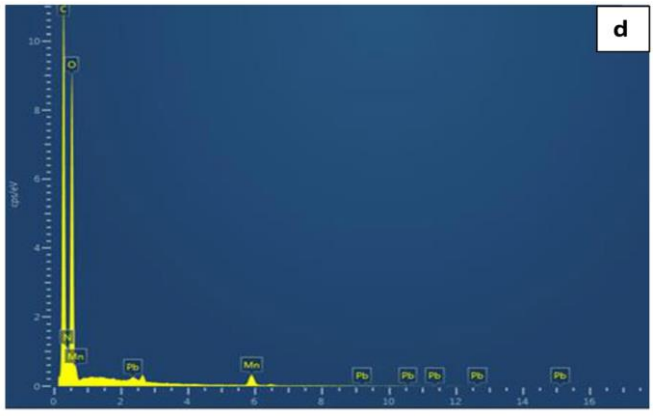

Fig. 6: Energy dispersive spectra of (d) Pb^{2+} doped LTMA single crystal

Table 6: EDX analysis of pure LTMA

Element	Line Type	Wt%	Atomic %
Carbon	K	41.51	49.7
Nitrogen	K	6.76	6.94
Oxygen	K	46.79	42.06
Manganese	K	4.94	1.29
Total:		100	100

Table 7: EDX results of (b) Zn^{2+} doped LTMA

Element	Line Type	Wt%	Atomic %
Carbon	K	36.47±0.19	51.73±0.26
Nitrogen	K	0.34±0.14	0.41±0.17
Oxygen	K	37.73±0.28 4	40.17±0.30
Manganese	K	21.24±0.22	6.59±0.07
Zinc	K	4.22±0.16	1.10±0.04
Total:		100	100

Table 8: EDX report of Cd^{2+} doped LTMA

Element	Line Type	Wt%	Atomic %
Carbon	K	38.65	48.04
Nitrogen	K	7.75	8.26
Oxygen	K	45.04	42.03
Manganese	K	3.85	1.05
Cadmium	L	4.70	0.62
Total:		100	100

Table 9: EDX results of Pb^{2+} doped LTMA

Element	Line Type	Wt%	Atomic %
Carbon	K	40.33	47.47
Nitrogen	K	9.14	9.22
Oxygen	K	48.55	42.9
Manganese	K	1.45	0.37
Lead	M	0.54	0.04
Total:		100	100

3.5. Optical Studies:

3.5.1. UV- Absorption & Transmittance analysis

The optical transmission spectra were recorded for the polished plates of the grown crystals using VARIAN CARY 5E UV-vis-NIR spectrophotometer. The spectrophotometer generates the monochromatic beam which resolves radiation into the corresponding wavelengths and the detector ensures the amount of beam transmitted through the sample. Two light sources are used to cover the entire range of spectrum (200-2500 nm). A straightened bandwidth was selected using band pass filters. The radiation was repeatedly passed with the cells. This double beam process eliminates the fluctuations on intensity of the scattered radiation and the solvent effects. The two beams were combined and difference in the intensities was calculated. The monochromator and recorder were compiled and adjusted so that the recording collected at the detector was maximum.

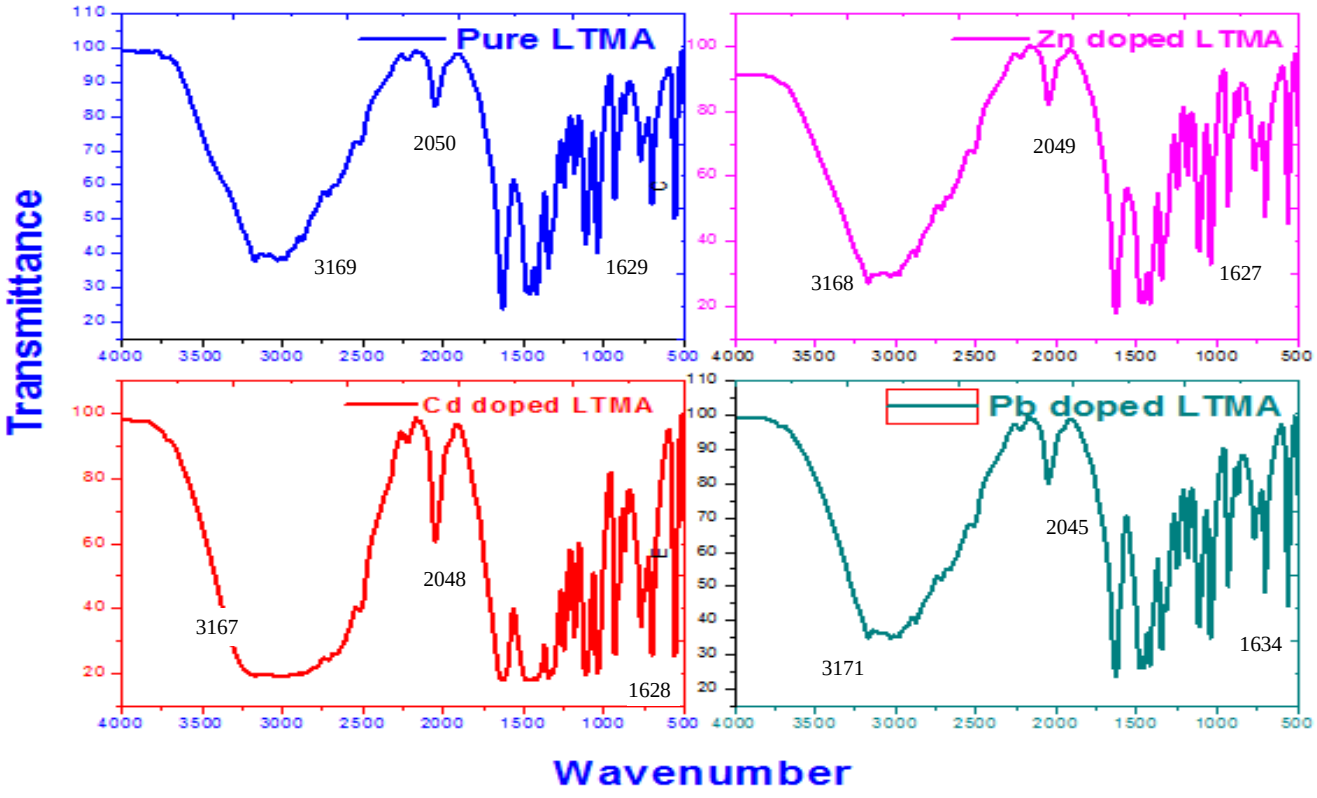

Fig. 7: FTIR Spectrum of pure LTMA and Zn^{2+}, Cd^{2+} and Pb^{2+} doped LTMA

The transmission study aimed to record the insensible beam in terms of percentage of transmittance along the y-axis and related wavelength (nm) along the x-axis. The UV-visible spectrum implies that the information is useful. The recorded UV-transmittance plots of the pure and doped LTMA crystals are shown in Fig. 5. The observed transmittance spectrum cutoff for both pure and doped crystals was obtained. UV absorption plot shows that the lower cutoff λ was ~267 nm and ~200 nm for the pure and doped crystals, respectively. The lower cutoff λ indicates the clear transparency, which confirms the use of this material in electro-optical devices, because the lower cutoff wavelength was 200 nm and this behavior can cause the NLO nature [25]. The energy band gap was calculated using formula for pure crystal as 4.6eV and for Zn^{2+}, Cd^{2+} and Pb^{2+} doped crystals as 6.3eV, 6.45eV and 6.5eV, respectively, which are shown in Fig. 6.

$$E_g=1240/\lambda \quad (3)$$

Table 10: FTIR Spectral assignment of pure LTMA and Zn^{2+}, Cd^{2+} and Pb^{2+} doped LTMA single crystal

Wavenumber Pure L-Threonine [Reported 14]	Pure LTMA	Zn^{2+} doped LTMA	Cd^{2+} doped LTMA	Pb^{2+} doped LTMA	Assignment
-	3169.25	3168.09	3167.43	3171	NH_3^+ asymmetric stretching
-	3029.80	3028.32	3027.75	3028.16	NH_3^+ symmetric stretching
1625.99	1629.28	1627.65	1628.20	1634	NH_3^+ asymmetric deformation
1417	1417.94	1417.16	1417.01	1413	NH_3^+ symmetric deformation
1346.48	1346.04	1345.48	1345.17	1343	CH symmetric deformation
--	1113.14	1112.73	1112.90	1112	NH_3^+ Rocking
1040.52	1040.72	1040.89	1040.62	1051	C-N Rocking
931.50	932.53	932.33	932.31	921	C-C Rocking
871.09	871.20	870.76	870.92	871.29	C-C-N Rocking
767.90	769.77	769.12	769.20	769.05	COO^- Bending
701.52	701.35	701.10	701.16	700	COO^- wagging vibration
560.19 C	560.11	559.90	559.85	549	COO^- Rocking Deformation
489.64	489.82	489.30	489.75	490.02	NH_3^+ Bending
-	445..18	444.79	445.36	445.89	In plan OCO Rocking

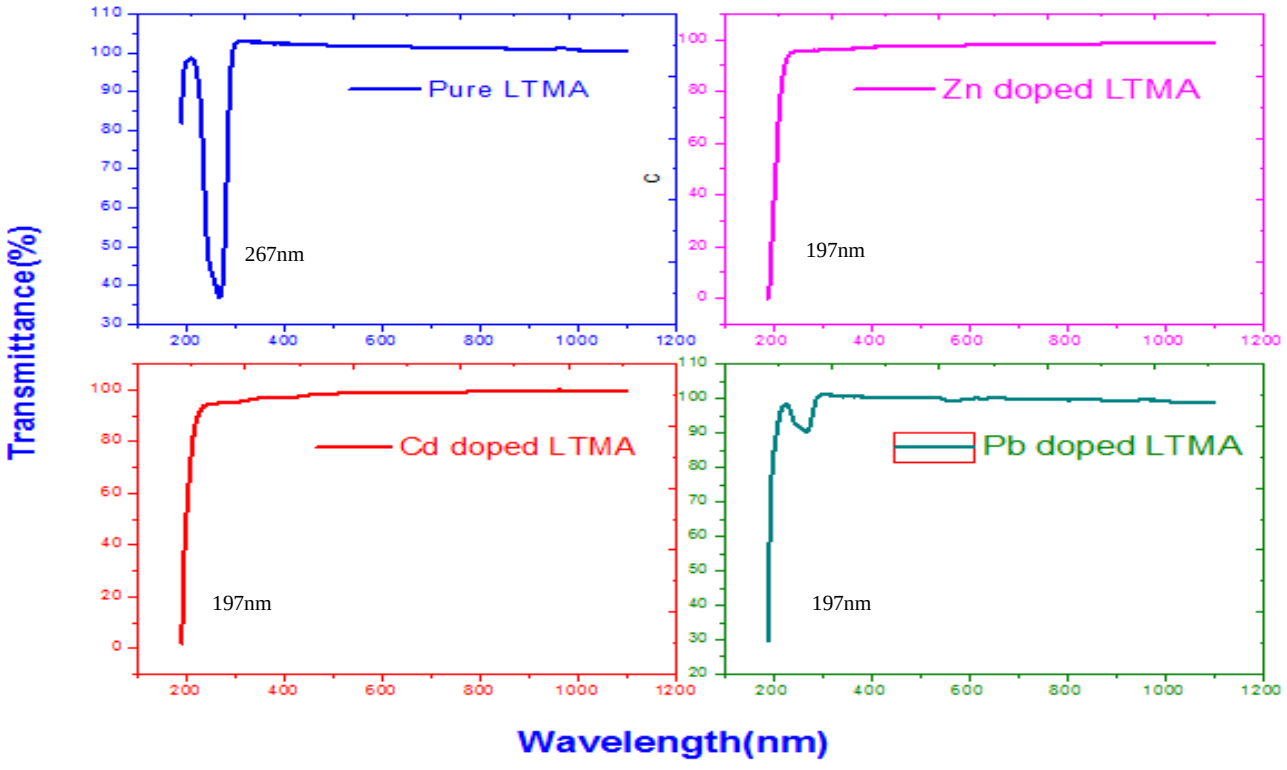

Fig. 8: The UV-visible transmittance spectra of pure and Zn^{2+}, Cd^{2+} and Pb^{2+} doped LTMA

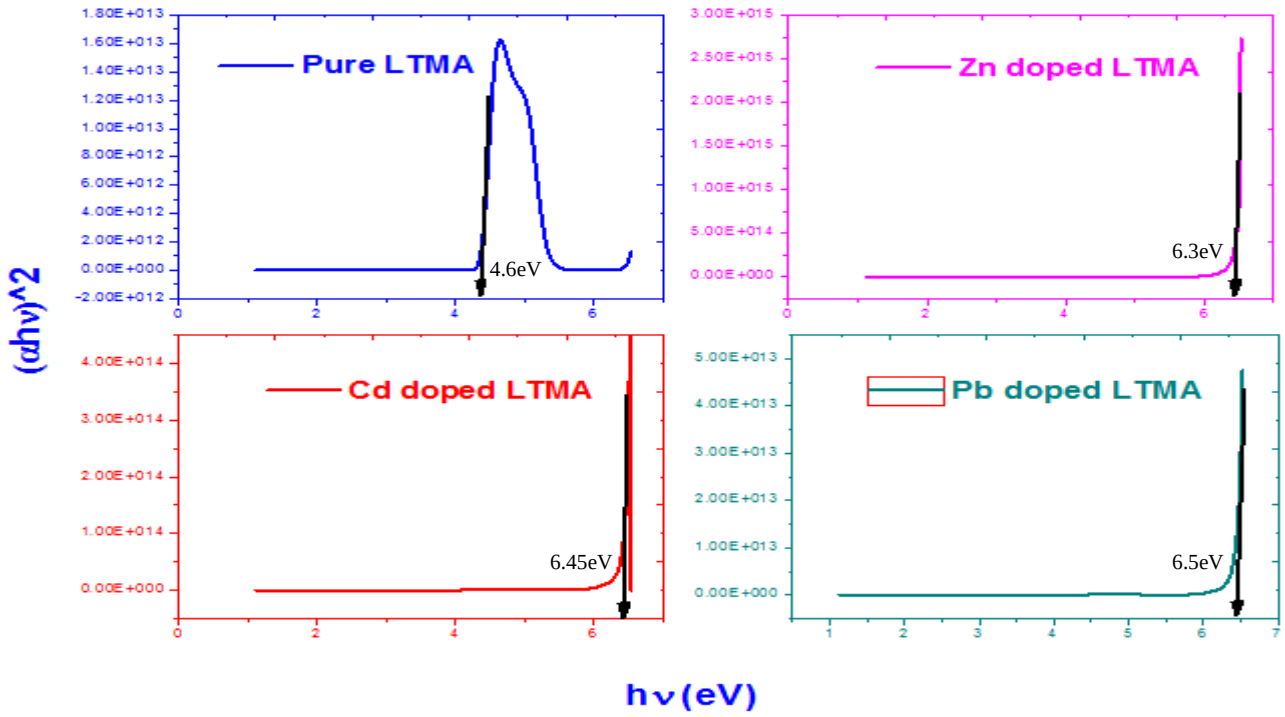

Fig. 9: Energy band gap spectra of pure and Zn^{2+}, Cd^{2+} and Pb^{2+} doped LTMA

3.6 Vicker's Microhardness Analysis

Microhardness study was obtained for determining the roughness of the grown crystals using HMT 2T, SHIMADZU. The indentation mark was determined for all the crystals at 30°C by applying loads of 25 gm, 50 gm and 100 gm. The hardness value H_v was found to be increasing with increase in mechanical stress applied from 25 gm to 100 gm and cracks were observed at the higher loads. Vicker's microhardness number H_v of the crystals was calculated using following equation:

$$H_v = 1.8544\ P/d^2\ (kg/mm^2) \quad (4)$$

Where, H_v-Vicker's hardness number in kg/mm^2, P – mechanical stress and d - average diagonal distance of the indentation. From the graph, it was shown that the hardness value of all the doped crystals increased with small bends up to 100 gm. So, all the hardness numbers of Zn^{2+}, Cd^{2+} and Pb^{2+} doped LTMA material were increased and the data is reported in table 11.

Table 11: Hardness values of pure LTMA and doped LTMA single crystals

Load (gm)	P	Hardness (H_V)			
		Pure LTMA	Zn^{2+} doped LTMA	Cd^{2+} doped LTMA	Pb^{2+} doped LTMA
25		37	29.34	27.6	29.85
50		50.8	40.8	30.2	49.65
100		80.5	57.7	43.35	78.6

3.7. Photoluminescence Study (PL)

The PL study of the grown LTMA and 0.2 M of Zn^{2+} doped LTMA, Cd^{2+} doped LTMA, Pb^{2+} doped LTMA crystals is shown in Fig. 10, which reveals the emission peak at 486.96 nm.

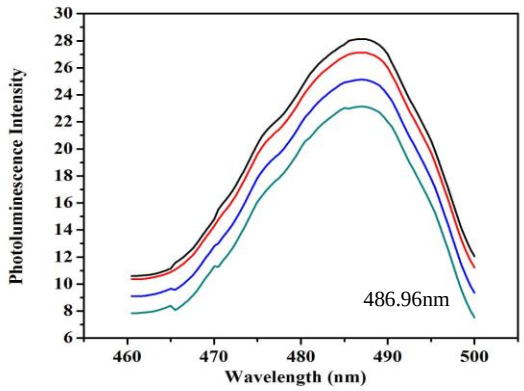

Fig. 10: PL spectrum of pure and doped LTMA crystal.

4. Conclusions

Novel single crystals of un-doped and inner doped L-threonine manganese acetate were effectively developed with spontaneous evaporation. EDX studies confirmed the presence of the dopant Mn in pure LTMA and doped

crystals. FTIR uncovered the nearness of utilitarian gatherings in the crystals. Enormous changes in mechanical quality of the pure and doped crystals were found by Vicker's micro hardness analyzer. PL emission spectrum wave length of 486.96 nm for the pure and doped LTMA crystals were also performed.

Acknowledgment

We express sincere thanks to SAIF, IIT-Madras, Tamil Nadu, India, SAIF, Cochin-Kerala, India and St. Joseph's College, Tiruchirappalli, Tamil Nadu, India, for their kind cooperation to complete this research work.

References

[1] M.L. Caroline and S. Vasudevan, "Growth and characterization of an organic nonlinear optical material" L-alanine alaninium nitrate, Materials Letters, vol. 62, pp. 2245-2248, (2008).

[2] S. Dhanuskodi and J. Ramajothi, "Crystal Growth, thermal and optical studies of L-Histidine Tetrafluoroborate-a Semi Organic NLO materials", Cryst. Res. Technol., vol. (39) 7, pp. 592–597, (2004)

[3] D. Eimerl, S. Velsko, L. Davis, F. Wang, J. Loiacono and F. Kennedy, "Deuterated L-Arginine phosphate: a new efficient nonlinear crystal", IEEE J. Quantum Electron, vol. 25, no. 2 , pp. 179-193, (1989).

[4] D. Geetha, M. Prakash, M.L. Caroline and P.S. Ramesh, "Growth and characterization of the nonlinear optical single crystal" L-Phenylalanine-benzoic acid, Adv. Appl. Sci. Res., vol. 2, no. 2, pp. 86-92, (2011).

[5] V. Ananthanarayanan, "Raman Spectra of Single Crystals of Zinc and Lithium Acetate Dihydrate", vol. 56, no. 4, pp. 188-197, (1962).

[6] T. Arii and A. Kishi, "The effect of humidity on thermal process of zinc acetate", Thermochimica Acta, vol. 400 no. 1-2, pp. 175-185, (2003).

[7] K. Arun and S. Jayalekshmi, "Growth and Characterization of Nonlinear Optical Single Crystals of L-Alaninium Oxalate", Journal of Minerals and Materials Characterization and Engineering, vol. 8, no. 8, pp. 635-646, (2009).

[8] T. Balakrishnan and K. Ramamurthi, "Growth and characterization of glycine lithium sulphate single Crystal", Crystal Research and Technology, vol. 41, no. 12, pp. 1184-1188, (2006).

[9] D. Balasubramanian, P. Murugakoothan and R. Jayavel, "Synthesis, growth and characterization of organic nonlinear optical bis-glycine maleate (BGM) single crystals", Journal of Crystal Growth, vol. 312, no. 11, pp. 1855-1859, (2010).

[10] J.H. Joshi, S. Kalainathan, D.K. Kanchan, M.J. Joshi and K.D. Parikh, "Effect of L-Threonine on growth and properties of ammonium dihydrogen phosphate crystal", Arabian Journal of Chemistry, vol. 13, pp. 1533-1550, (2020).

[11] S.M. Britto Dhas, M. Suresh, P. Raji, K. Ramachandran and S. Natarajan, "Photoacoustic studies on two new organic NLO materials: L-threonine and L-prolinium tartrate", Crystal Research and Technology, vol. 42, no. 2, pp. 190-194, (2007).

[12] S. Gunasekaran and G.R. Ramkumar, "Analysis on Suitability of Pure and α-Histidine Doped KDP Crystals in High Speed Applications", Indian Journal of Physics, vol. 83, pp. 1549, (2009).

[13] C.S. Hwang, N.R. Lee, Y.A. Kim and Y.B. Park, "Synthesis of the Water Dispersible L-Valine Capped ZnS: Mn Nano crystal and the Crystal Structure of the Precursor Complex: $Zn(Val)_2(H_2O)$", Bull. Korean Chem. Soc., vol. 27. No. 11, pp. 1809-1814, (2006).

[14] G.R. Kumar, S.G. Raja, R. Mohana and R. Jayavel, "Growth, structural and spectral analyses of nonlinear optical L-Threonine single crystals", Journal of Crystal Growth, vol. 275, pp. 1947-1951, (2005).

[15] N. Indumathi, K. Deepa and S. Senthil, "Growth and characterization of L-Threonine Lithium Chloride: A New semi organic Non Linear Optical single crystal", IJEDR, vol. 8, no. 1, pp. 560-564, (2017).

[16] R. Vivekanandhan, K. Raju, S. Sahaya Jude Dhas and V. Chidambaram, "Investigation of Novel Nonlinear Optical L-Threonine Calcium Chloride Single Crystal Grown by Solution Growth Technique", International Journal of Applied Engineering Research, vol. 13, no. 18, pp. 13454-13459, (2018).

[17] S. Masilamani, A.M. Musthafa and P. Krishnamurthi, "Synthesis, growth and characterization of a semiorganic nonlinear optical material: L-Threonine Cadmium Chloride single crystals", vol. 10, no. 2, pp. S3962-S3966, (2017).

[18] C. Vijayaraj, M. Mariappan, G. Nedunchezhian, D. Benny Anburaj and B. Gokulakumar, "Synthesis Growth and Characterization of a New NLO Material: L-Threonine Manganese Chloride" Indo–Asian Journal of Multidisciplinary Research (IAJMR), vol. 2, no. 2, pp. 555-560, (2018).

[19] J. Elberin Mary Theras, D. Kalaivani, J. Arul Martin Mani, D. Jayaraman and V. Joseph, "Synthesis, structural and optical properties, ferromagnetic behaviour, cytotoxicity and NLO activity of lithium sulphate doped L-Threonine", Optics & Laser Technology, vol. 83, pp. 49-54, (2016).

[20] T. Manimaran, P. Paramasivam, S. Bhuvaneswari, R.S. Abina Shiny, B. Ravindran and M. Mariappan, "Growth and Characterization of L-Threonine Potassium Sulphate" A New NLO Semi Organic Crystal, Research Review Journal, vol. 4, no. 03, pp. 644-647, (2019).

[21] S.A.D. Christopher and N.N.K. Pillai, "Growth and Structural studies of Zn doped L-Threonine single crystal", IJES, vol. 4, no. 8, pp. 1-4, (2015).

[22] M. Nagarajan, N.N. Pillai, S. Perumal, "Growth and Structural studies of Cu doped L-Threonine single crystal", IJLTEMAS, vol. IV. no. XI, pp. 7-11, (2015).

[23] M.A. Jeba Queen, K.C. Bright, S.M. Delphine, and P.A. Udhaya, "Spectroscopic Investigation of supramolecular organometallic compound L-Threonine Cadmium Acetate Monohydrate", Spectrochemica Acta, Part A: Molecular and Biomolecular Spectroscopy, vol. 19, pp. S1386-1425, (2019).

[24] A. Puhal Raj and C. Ramachandra Raja, "Synthesis, Growth, Structural, Spectroscopic, Thermal and Optical Properties of NLO Single Crystal L-Threonine Zinc Acetate", Photonics and Optoelectronics (P&O), vol. 3, pp. 56-64, (2013).

[25] K. Sudhakar, S. Muniyappan and P. Murugakoothan, "Growth and Characterization of a Potential Organic NLO Single Crystal: Guanidinium 4-Aminobenzene Sulfonate (GuAS)", materials today: Proceedings, vol. 8, no. 1, pp. 256-263, (2019).